Article

Isoreticular Metal−Organic Frameworks Confined Mononuclear Ru-Hydrides Enable Highly Efficient Shape-Selective Hydrogenolysis of Polyolefins

Manav Chauhan, Neha Antil, Bharti Rana, Naved Akhtar, Chhaya Thadhani, Wahida Begum, and Kuntal Manna*

Cite This: JACS Au 2023, 3, 3473−3484

Read Online

ACCESS | Metrics & More | Article Recommendations | SI Supporting Information

ABSTRACT: Upcycling nonbiodegradable plastics such as polyolefins is paramount due to their ever-increasing demand and landfills after usage. Catalytic hydrogenolysis is highly appealing to convert polyolefins into targeted value-added products under mild reaction conditions compared with other methods, such as high-temperature incineration and pyrolysis. We have developed three isoreticular zirconium UiO-metal−organic frameworks (UiO-MOFs) node-supported ruthenium dihydrides (UiO-RuH$_2$), which are efficient heterogeneous catalysts for hydrogenolysis of polyethylene at 200 °C, affording liquid hydrocarbons with a narrow distribution and excellent selectivity via shape-selective catalysis. UiO-66-RuH$_2$ catalyzed hydrogenolysis of single-use low-density polyethylene (LDPE) produced a C12 centered narrow bell-shaped distribution of C8−C16 alkanes in >80% yield and 90% selectivity in the liquid phase. By tuning the pore sizes of the isoreticular UiO-RuH$_2$ MOF catalysts, the distribution of the products could be systematically altered, affording different fuel-grade liquid hydrocarbons from LDPE in high yields. Our spectroscopic and theoretical studies and control experiments reveal that UiO-RuH$_2$ catalysts enable highly efficient upcycling of plastic wastes under mild conditions owing to their unique combination of coordinatively unsaturated single-site Ru-active sites, uniform and tunable pores, well-defined porous structure, and superior stability. The kinetics and theoretical calculations also identify the C−C bond scission involving β-alkyl transfer as the turnover-limiting step.

KEYWORDS: MOFs, hydrogenolyis, polyolefins, ruthenium dihydrides, low-density polyethylene
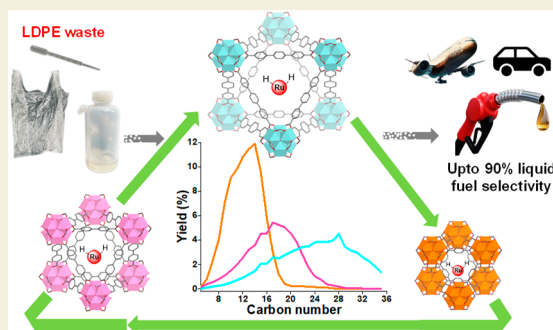
INTRODUCTION

With an estimated valuation of USD 609 billion in 2022, the global plastics market is expected to grow further.[1] The usage of single-use plastics for gloves, personal protective equipment, masks, and food packaging has increased in the post-COVID era. With almost 400 million metric tons of plastic being generated annually,[2] polyolefins such as polyethylene and polypropylene contribute about 60% of that total, and nearly 80% of these end up in landfills or oceans.[3] The strong sp^3 carbon−carbon covalent bonds in polyolefins increase the stability and durability; however, they also induce difficulties in the degradation and upcycling of the plastics.[4] Popular methods of utilizing plastic waste involve energy-intensive incineration[5−7] and pyrolysis,[8−10] where the plastic waste is heated at 800−1200 °C in the presence or absence of oxygen to generate heat or liquid oil, syngas, and char, respectively. However, the requirement of high temperature, emission of greenhouse gases and hazardous toxins, and lack of control over product selectivity make these processes environmentally and economically unviable at a massive scale.

Catalytic hydrogenolysis of polyolefins offers an attractive pathway for controlling product selectivity under milder reaction conditions in converting polyolefins to targeted value-added products.[11] Dufaud and Basset reported the hydrogenolysis of polyethylene and polypropylene to diesel or lower alkanes using a silica−alumina supported zirconium hydride catalyst.[12] Recently, several heterogeneous catalysts, such as Pt/C,[13] Pt/SrTiO$_3$,[14,15] mSiO$_2$/Pt/SiO$_2$,[16] Pt/Al$_2$O$_3$,[17] Ru/C,[18−21] Ru/CeO$_2$,[22] Ru/TiO$_2$,[23] and Ru/ZrO$_2$[24] have also been developed for such transformations under relatively mild conditions. However, these nanoparticle-based catalytic systems contain a high-loading of precious metals and multiple active sites that lead to the formation of liquid and gaseous hydrocarbons with a broad distribution due to the random C−
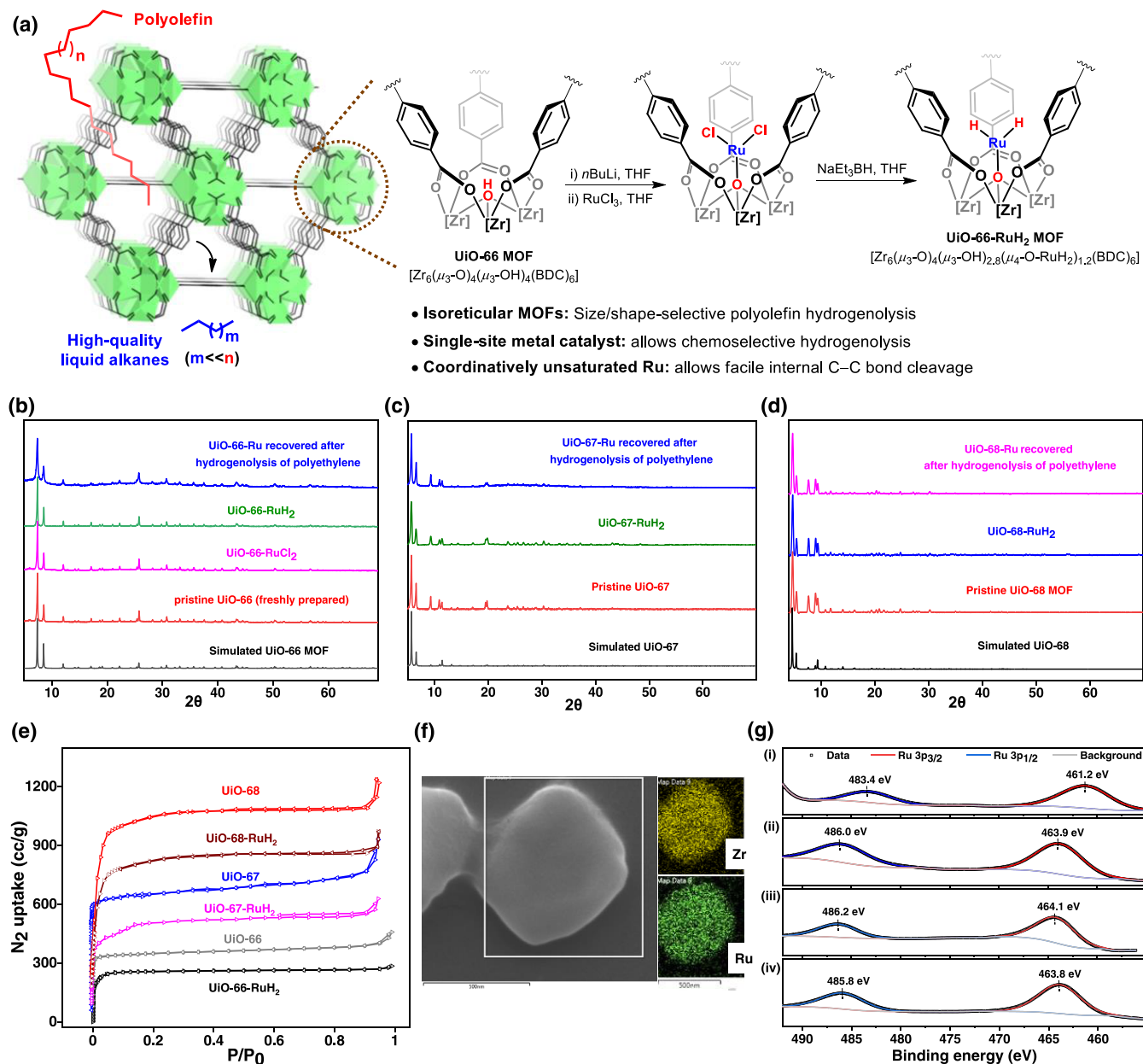
Figure 1. (a) Synthesis of UiO-66-RuH$_2$ via postsynthetic metalation of the UiO-66 MOF. (b) PXRD patterns of the simulated UiO-66 MOF (black), pristine UiO-66 (red), UiO-66-RuCl$_2$ (magenta), UiO-66-RuH$_2$ (green), and UiO-66-Ru recovered after the hydrogenolysis of polyethylene (blue). (c) PXRD patterns of the simulated UiO-67 MOF (black), pristine UiO-67 (red), UiO-67-RuH$_2$ (green), and UiO-67-Ru recovered after the hydrogenolysis of polyethylene (blue). (d) PXRD patterns of the simulated UiO-68 MOF (black), pristine UiO-68 (red), UiO-68-RuH$_2$ (blue), and UiO-68-Ru recovered after the hydrogenolysis of polyethylene (magenta). (e) N$_2$ sorption isotherms (77 K) of UiO-66 (gray), UiO-66-RuH$_2$ (black), UiO-67 (blue), UiO-67-RuH$_2$ (magenta), UiO-68 (red), and UiO-68-RuH$_2$ (maroon). (f) SEM image of a UiO-66-RuH$_2$ particle along with the elemental mapping of Zr and Ru. (g) Ru 3p XPS spectra of (i) Ru(0)-nanoparticles@UiO-66, (ii) RuCl$_3$·3H$_2$O (iii) UiO-66-RuCl$_2$, and (iv) UiO-66-RuH$_2$.

C bond cleavage.[25] Moreover, many such catalysts suffer from difficulty in controlling the sizes of metal nanoparticles and nonuniform pore surfaces and require preactivation at high temperatures.

Shape-selective catalysts such as ZSM-5, zeolites, and silicalite-1 are widely used in the petroleum industry for isomerization of hydrocarbons, dehydration reactions and production of synthetic gasoline, owing to their uniform pore structure, high thermal stability, and high concentration of active sites.[26−35] Huang and Sadow recently reported the pore template effect on the overall distribution of products in the

hydrogenolysis of polyolefins using a platinum nanoparticle catalyst embedded in mesoporous silica shell supported on a solid silica sphere, mSiO$_2$/Pt-Size/SiO$_2$.[36] We envisioned that developing single-site metal catalysts within porous materials having uniform and tunable pores would better control the C−C bond cleavage and product selectivity during the hydrogenolysis of polyolefins via shape-selective catalysis.

As porous and tunable molecular material, metal−organic frameworks (MOFs) have drawn immense interest for developing single-site heterogeneous catalysts for various applications.[37−71]
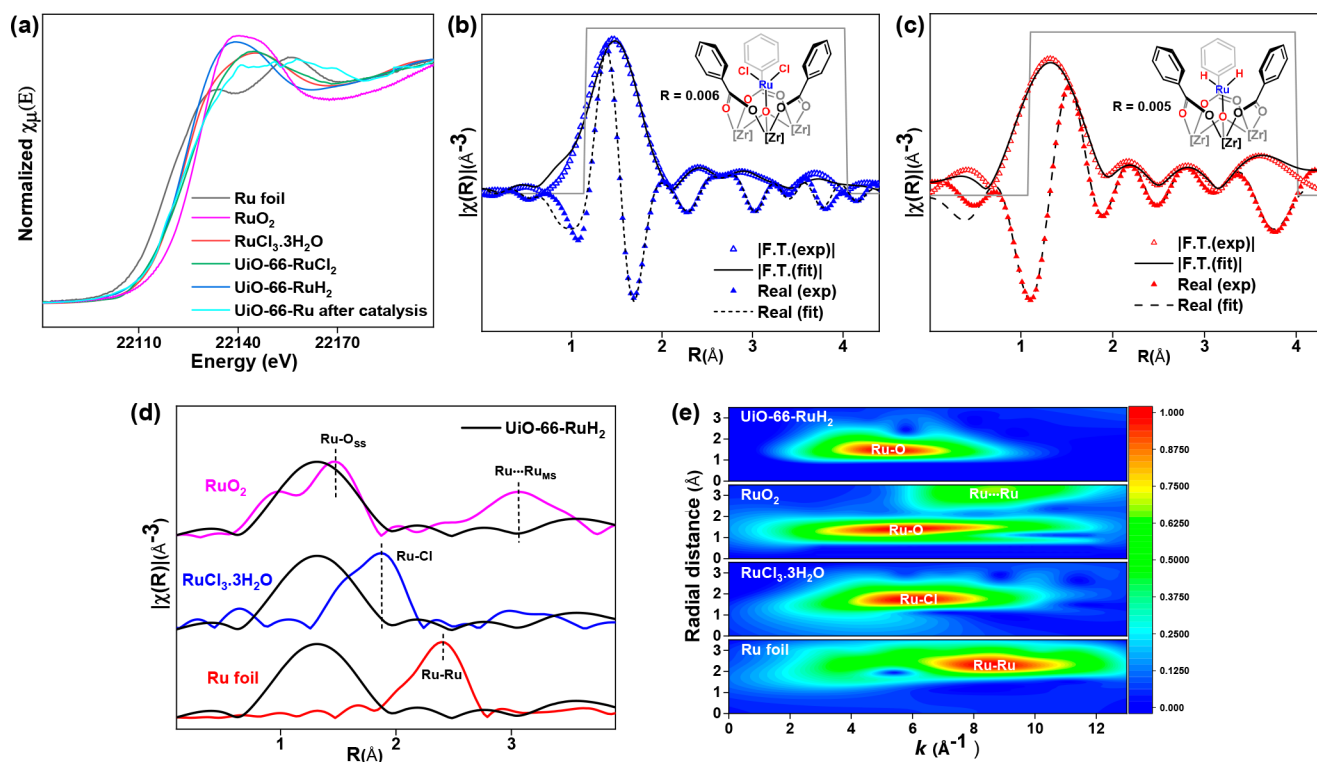
Figure 2. (a) Ru K-edge XANES spectra of Ru foil (black), RuO$_2$ (magenta), RuCl$_3$·3H$_2$O (red), UiO-66-RuCl$_2$ (green), UiO-66-RuH$_2$ (blue) and UiO-66-Ru after hydrogenolysis (4 μmol of Ru) of 0.6 g of polyethylene at 200 °C for 72 h under 35 bar H$_2$ pressure (turquoise). (b) EXAFS spectra (blue solid and hollow triangles) and fits (black solid and dashed lines) of UiO-66-RuCl$_2$ in the R space at the Ru K-edge. The fitting range in the R space is 1.1–4 Å. (c) EXAFS spectra (red solid and hollow triangles) and fits (black solid and dashed lines) of UiO-66-RuH$_2$ in the R space at the Ru K-edge. The fitting range in the R space is 1.1–4 Å. (d) k^2-weighted Ru-EXAFS χ(R) spectra of UiO-66-RuH$_2$ (black), Ru foil (red), RuCl$_3$·3H$_2$O (blue), and RuO$_2$ (magenta). (e) Wavelet transform for the k^2-weighted EXAFS signal at the Ru K-edge.

Owing to their isoreticular nature, ease of tunability of pores, uniform porous and crystalline structures, MOFs have also been employed for size- or shape-selective catalysis.[72−76] Notably, the metal oxo cluster-based secondary-building units (SBUs) of MOFs, resembling tiny metal-oxide clusters, offer unique oxide support for developing single-site metal catalysts via active-site isolation.[77−88] We herein present a state-of-the-art catalytic architecture comprising single-site ruthenium hydride catalysts supported by the SBUs of isoreticular Zr-UiO-MOFs for shape-selective hydrogenolysis of polyolefins. Zr-UiO-MOFs, constructed from Zr$_6$O$_4$(OH)$_4$ SBUs bridged by linear dicarboxylate linkers, have *fcu* topology and excellent thermal and chemical stability.[89] We demonstrate that because of the unique combination of single-site nature and uniform porous structure, UiO-RuH$_2$ catalysts enable efficient hydrogenolysis of polyethylene into short-chain hydrocarbons with a narrow distribution. By tuning the pore sizes of the isoreticular UiO-RuH$_2$ MOF catalysts, the distribution of the products could be systematically altered, affording different fuel-grade liquid hydrocarbons with narrow alkane distributions from the single-use polyethylene in high yields.

■ RESULTS AND DISCUSSION

Synthesis and Characterization of Isoreticular UiO-MOF Node Supported Ru-Dihydrides (UiO-66-RuH$_2$, UiO-67-RuH$_2$, and UiO-68-RuH$_2$)

Three isoreticular MOF-supported Ru-dihydrides, UiO-66-RuH$_2$, UiO-67-RuH$_2$, and UiO-68-RuH$_2$, were synthesized by postsynthetic metalation of the nodes of the corresponding

freshly prepared UiO-66, UiO-67, and UiO-68 MOFs. UiO-MOFs, having 3D porous UiO-topology, are constructed from Zr$_6$O$_4$(OH)$_4$ nodes interconnected with linear dicarboxylate bridging linkers.[89,90] The treatment of UiO-MOFs with *n*-BuLi in THF to deprotonate the μ_3-OH groups at the nodes followed by reaction with RuCl$_3$ in THF at room temperature afforded the corresponding UiO-RuCl$_2$. Subsequently, the reaction of UiO-RuCl$_2$ and NaEt$_3$BH in THF furnished the corresponding UiO-RuH$_2$ via chloride-hydride exchange at the Ru ion. The Ru-loadings with respect to the μ_3-OH group in UiO-66-RuH$_2$, UiO-67-RuH$_2$, and UiO-68-RuH$_2$ were found as 30%, 35%, and 33%, respectively, as determined by inductively coupled plasma optical emission spectroscopy (ICP-OES) analysis of the digested MOFs. The similarity of the powder X-ray diffraction (PXRD) pattern between UiO-RuCl$_2$, UiO-RuH$_2$, and the corresponding pristine UiO-MOF indicated the retention of the crystallinity and structure of the MOFs during postsynthetic treatments (Figure 1b−d).[89,91] UiO-66-RuH$_2$, UiO-67-RuH$_2$, and UiO-68-RuH$_2$ had a BET surface area of 903 m^2/g, 1420 m^2/g, and 2300 m^2/g, and the corresponding pore sizes are 5.1, 6.8, and 8.1 Å, respectively (Figure 1e). A characteristic ν_{Ru-H} stretching frequency of UiO-66-RuH$_2$ was observed at 1980 cm^{-1} in the Infrared spectrum (KBr) (Figure S4, SI). Scanning electron microscopy (SEM) energy-dispersive X-ray (EDX) mapping of UiO-66-RuH$_2$ indicated that Ru and Zr are uniformly dispersed throughout the MOF particles (Figure 1f). The X-ray photoelectron spectroscopy (XPS) spectra of UiO-66-RuCl$_2$ and UiO-66-RuH$_2$ confirmed the +4 oxidation state of zirconium ion at MOF nodes (Figures S28 and S29). Due to
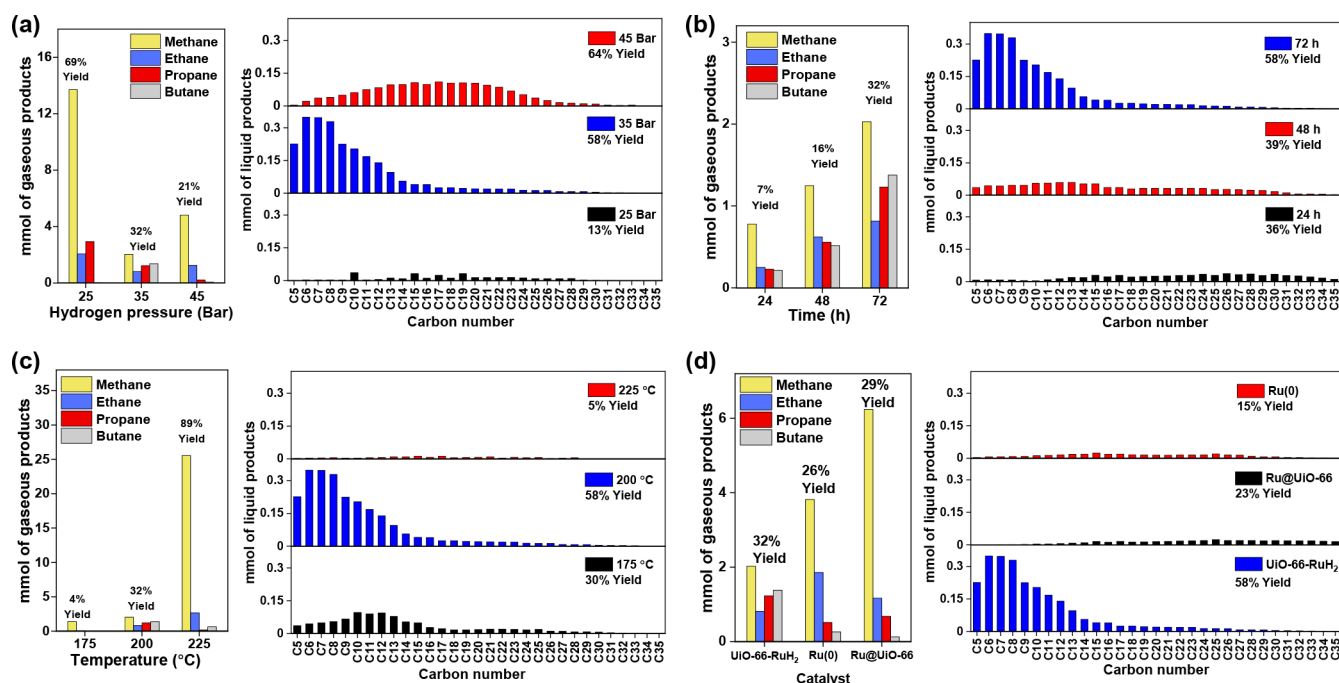
Figure 3. Optimization of reaction conditions for the hydrogenolysis of 0.60 g of polyethylene ($M_w \sim 4000$ Da, $M_n \sim 1700$ Da). (a) Effect of the pressure on the overall product yields. Reaction conditions: 6 mg UiO-66-RuH$_2$ (4 μmol of Ru), 200 °C, and 72 h. (b) Effect of time on overall product yields. Reaction conditions: 6 mg of UiO-66-RuH$_2$ (4 μmol of Ru), 200 °C, and 35 bar H$_2$. (c) Effect of temperature on overall product yields. Reaction conditions: 6 mg of UiO-66-RuH$_2$ (4 μmol of Ru), 35 bar of H$_2$, and 72 h. (d) Control experiments with Ru(0)-nanoparticles and Ru(0)@UiO-66. Reaction conditions: $\sim$ 4 μmol of Ru, 35 bar H$_2$, 200 °C, and 72 h.

the overlap of the 3d binding energy of ruthenium at 285 eV with the carbon 1s at 284.8 eV, the oxidation state of Ru was assigned by its 3p binding energies. The Ru$_{3p3/2}$ and Ru$_{3p1/2}$ binding energies of UiO-66-RuH$_2$ at 463.8 and 485.8 eV, respectively, suggested a +3 oxidation state of Ru. These binding energies are close to those of RuCl$_3$.3H$_2$O and UiO-66-RuCl$_2$, and $\sim$2.5 eV higher than Ru(0)-nanoparticles@ UiO-66.[92]

The +3 oxidation of Ru in UiO-66-RuCl$_2$ and UiO-66-RuH$_2$ was further confirmed by their X-ray absorption near-edge structure (XANES), which showed that Ru K-edge energies at $\sim$22,118 eV were closer to that of RuCl$_3$.3H$_2$O and $\sim$1.6 eV lower to RuO$_2$ (Figure 2a). The extended X-ray adsorption fine structure (EXAFS) of UiO-66-RuCl$_2$ at the Ru K-edge fitted well with the DFT optimized structure suggests that Ru^{3+} is coordinated with two chlorine atoms and one μ_4-O$^-$ and is equidistant from the six neutral carboxylate oxygens present at the node (Figure 2b). Fitting the Ru K-edge EXAFS data of UiO-66-RuH$_2$ with its DFT-optimized structure revealed a similar coordination environment of the Ru^{3+} ion (Figure 2c). At the UiO-66-RuH$_2$ node, Ru is coordinated with μ_4-O$^-$ and two hydrides with a corresponding Ru−O bond distance of 1.80 Å. To check the potential existence of any Ru nanoparticles in UiO-66-RuH$_2$ that might be formed during the treatment of NaEt$_3$BH, we examined the fitting of the experimental EXAFS spectrum of UiO-66-RuH$_2$ to its DFT model with different percentages (5−80%) of metallic Ru (Figure S27, SI). These EXAFS analyses showed significant misfits and higher R-factors, which indicated the absence of metallic Ru nanoparticles in UiO-66-RuH$_2$. This is further reinstated by the absence of the Ru···Ru scattering feature of Ru foil at 2.38 Å in the phase uncorrected k^2-weighted Ru-EXAFS χ(R) of UiO-66-RuH$_2$ (Figure 2d). In this spectrum,

the first scattering peak centered at $\sim$1.4 Å is due to the Ru−O single scattering, similar to that of RuO$_2$, and the second weak scattering at 2.25 Å is attributed to the Ru−O$_{carboxylate}$ multiple scattering (Figure 2d). However, Ru···Ru multiple scattering features of RuO$_2$ at 3.3 Å is absent in the EXAFS of UiO-66-RuH$_2$. In addition, the k^2-weighted wavelet transform of the Ru atom of Ru foil showed Ru···Ru scattering at a k-value of 9 Å^{-1}, which is absent in both UiO-66-RuH$_2$ and UiO-66-RuCl$_2$ (Figure 2e and S26, SI). The only significant scattering of UiO-66-RuH$_2$ was observed at $\sim$6 Å^{-1}, corresponding to the Ru−O single scattering. These EXAFS features and wavelet trans-formed plot suggest the existence of only isolated Ru^{3+} ions at the node of UiO-66-RuH$_2$, which has no Ru-neighbors.

Hydrogenolysis of Polyethylene on UiO-66-RuH$_2$ Catalyst

UiO-66-RuH$_2$ is an active catalyst for the hydrogenolysis of polyethylene using H$_2$. The hydrogenolysis of polyethylene was first optimized using 0.60 g of polyethylene [weight-average molecular weight (M_w) $\sim$ 4000 Da, number-average molecular weight (M_n) $\sim$ 1700 Da] and 6 mg of UiO-66-RuH$_2$ (4 μmol Ru) in a high-pressure batch reactor with varying amount of H$_2$, temperature and time. After the reaction, the gaseous and liquid products were identified by gas chromatog-raphy (GC)-mass spectrometry (MS) and quantified via a GC-flame ionization detector (FID). Heating a mixture of polyethylene and UiO-66-RuH$_2$ for 72 h at 200 °C under 25 bar H$_2$ produced a mixture of gaseous (C1−C4) and liquid (C5−C20) hydrocarbons in $\sim$5:1 weight ratio and 82% conversion of polyethylene (Figure S13, SI). However, when the pressure was increased to 35 bar, the weight ratio of gaseous to liquid hydrocarbons dropped to 1:1.8, favoring the formation of more liquid products with 90% conversion (Figure 3a).
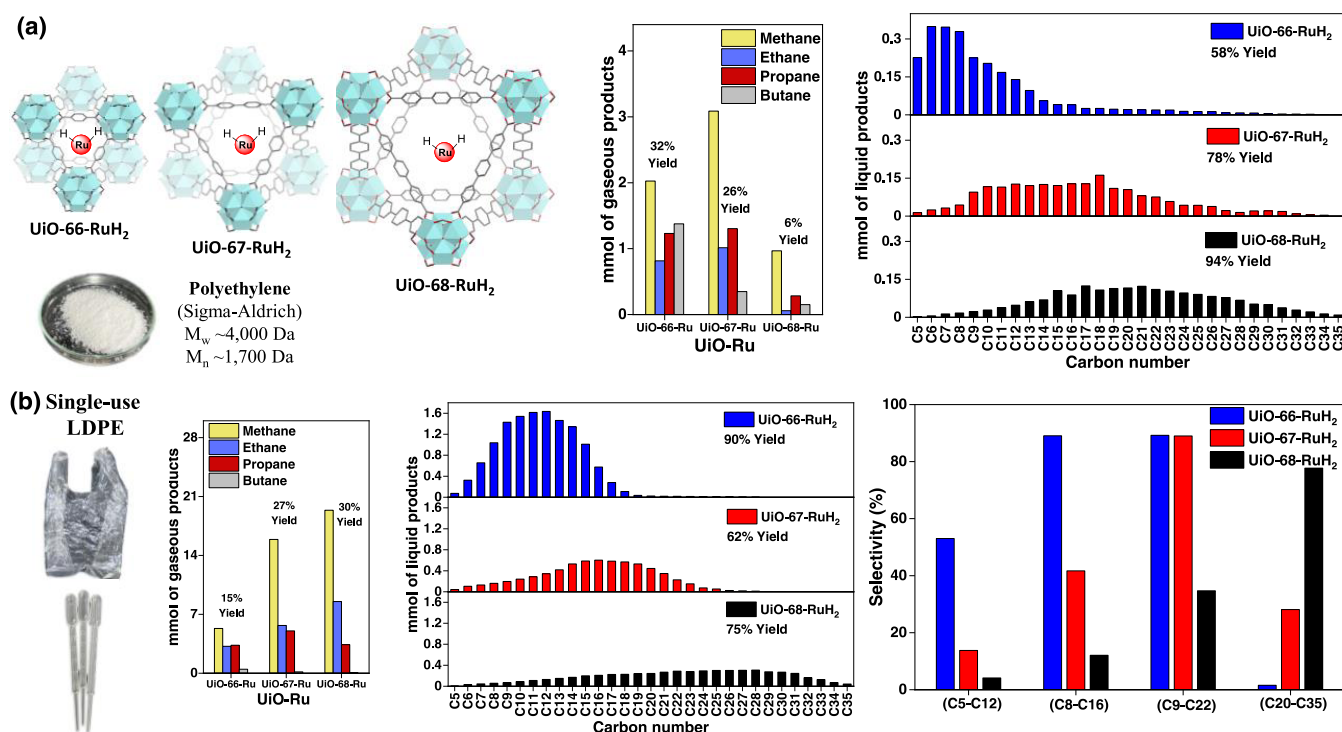
Figure 4. (a) Hydrogenolysis of commercially available polyethylene by differently pore sized UiO-Ru to afford liquid and gaseous products. Reaction conditions: 0.60 g of polymer substrate, $\sim$ 4 μmol of Ru, 200 °C, 35 bar H_2 and 72 h. (b) Hydrogenolysis of postconsumer single-use LDPE plastic bags or droppers by different pore sized UiO-Ru to afford liquid and gaseous products along with %selectivity of liquid products in several alkane ranges. Reaction conditions: 2.4 g of polymer substrate, $\sim$ 16 μmol of Ru, 200 °C, 35 bar H_2, and 20 h.

This ratio further diminished to 1:3 during the hydrogenolysis under 45 bar H_2, which suggests that the terminal cleavage of the C−C bonds suppresses, while the midscission of C−C bonds dominates at higher H_2 pressure. The product distribution in the UiO-66-RuH$_2$ catalyzed hydrogenolysis of polyethylene also varied significantly with the pressure of H_2. The liquid alkanes obtained under 35 bar H_2, were 66% selective in C5−C12 alkanes, while liquid products under 45 bar H_2 had 75% selectivity for C9−C22 alkanes (Figure 3a). Next, time-dependent hydrogenolysis was performed following the same methods under 35 bar of H_2 at 200 °C. A broad distribution of C11−C35 chains was formed in 43% polyethylene conversion after 24 h reaction. Hydrogenolysis in longer reaction time not only increased the conversion of PE, but also shifted the distribution of C_n chains in the liquid products toward lower alkanes. At the same time, the production of propane and butane dominates over that of methane in the gaseous phase (Figure S14, SI). The PE deconstruction also significantly depends on the reaction temperature. Upon increasing the temperature from 175 to 225 °C under 35 bar H_2 pressure for 72 h, the conversion of PE rose from 34% to 94%, and the gas-to-liquid product ratio increased from almost 1:7 to 18:1 due to the faster C−C bond scission at the higher temperature. The production of methane increased drastically at a temperature above 200 °C due to overhydrogenolysis, and in fact, 72% of methane was formed at 225 °C with approximately 5% liquid conversion of polyethylene (Figure 3c). Overall, the high yield of liquid hydrocarbons with narrow C_n-distribution was afforded during the hydrogenolysis of PE at 200 °C under 35 bar of H_2 pressure.

Effect of Pore Sizes of Isoreticular UiO-RuH$_2$ MOFs on Product Distribution and Selectivity

The pore sizes of the MOFs significantly influenced the identity of the products. The C_n-product distribution of the hydrogenolysis of polyethylene ($M_w \sim$ 4000 Da, $M_n \sim$ 1700 Da) under the optimized conditions using isoreticular UiO-RuH$_2$ MOFs is displayed in Figure 4a. A gradual shift of the liquid products from a lower and narrow product range to a higher and broader product range was observed with increasing pore sizes of the MOF catalysts. The highest selectivity of a particular Cn-range obtained in the liquid phase was 66% in C5−C12 alkanes for UiO-66-RuH$_2$, 74% in C8−C22 alkanes for UiO-67-RuH$_2$, and 68% in C20−C35 alkanes (lubricants) for UiO-68-RuH$_2$. Notably, the yield of gaseous products falls to as low as 6% for UiO-68-RuH$_2$, making it a very selective MOF for hydrogenolysis into 94% liquid products (Figure 4a).

Next, we tested the catalytic activity of UiO-Ru MOFs for hydrogenolysis of real-world postconsumer single-use plastic grocery bags or droppers made of low-density polyethylene [LDPE; Mw $\sim$ 150 kDa, determined by Gel Permeation Chromatography (GPC)]. Initial reaction conditions were LDPE (0.60 g), UiO-RuH$_2$ (4 μmol Ru) and 35 bar of H_2 in a high-pressure autoclave, heated at 200 °C for 72 h. Despite the intricacy of the LDPE's structure and absenteeism of any pretreatment, the UiO-RuH$_2$ catalysts almost completely converted the plastics bag into small chain liquid hydrocarbons in 56−89% yields (Figure S17, SI). UiO-66-RuH$_2$, owing to its smallest pore size of 5.1 Å, provided a C12-centered narrow bell-shaped distribution of chain lengths, affording C8−C16 or C9−C22 alkanes in 89% yield over 90% liquid product selectivity. The GC-FID analysis of the gaseous products showed an almost even distribution of methane, ethane, and

propane, with a total gas conversion of only 14% (Figure S17, SI). Interestingly, scaling up the catalytic reaction by 4-fold with the same LDPE to Ru weight ratio of 1485, led to the significant shorting of the reaction time from 72 to 20 h with almost similar yield and distribution (Figure 4b), which was attributed to the better diffusion of the molten LDPE within MOFs. Upon decreasing the LDPE to Ru weight ratio to 742, complete conversion of LDPE was achieved in 8 h with 88% liquid product yield. Under the optimized reaction condition with LDPE to Ru weight ratio of 1485, the hydrogenolysis of LDPE plastic bag using UiO-67-RuH$_2$ also produced liquid hydrocarbons as the major products containing a C16-centered distribution of carbon chains (Figure 4b). However, this product distribution slightly shifted toward the longer chains compared to that obtained using UiO-66-Ru catalyst, affording C9−C22 alkanes in 89% liquid product selectivity. In all of these cases, the amount of branched alkanes in the liquid product was ∼3−4% as estimated by GCMS analysis. UiO-68-RuH$_2$, having the larger pore sizes, converted ∼75% of the LDPE plastic bag into short-chain liquid hydrocarbons, which had a wider distribution and contained about 78% C20−C35 (lubricants) alkanes (Figure 4b). Moreover, UiO-67-Ru could be recycled and reused at least five times without any apparent drop-in catalytic activity and selectivity (Figure 5). The MOF
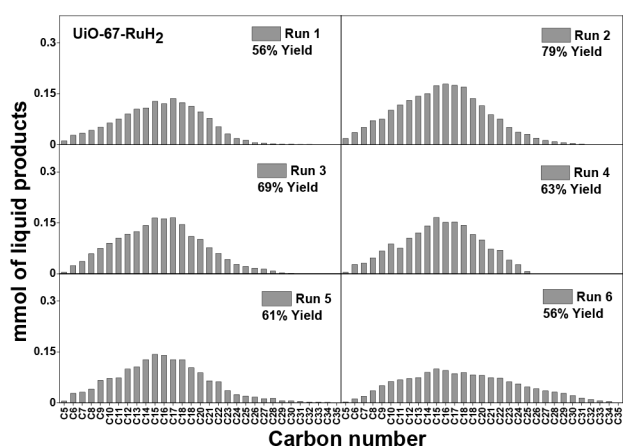
Figure 5. Liquid product distribution of hydrogenolysis of postconsumer LDPE plastic bag using UiO-67-RuH$_2$ for 6 consecutive runs. Reaction conditions: 0.60 g of polymer substrate in each run, 6.5 mg of UiO-67-RuH$_2$ (4 μmol of Ru), 200 °C, 35 bar H$_2$, and 72 h.

structure remained intact during the recycling, as evident by the PXRD of the recovered UiO-67-Ru after each run (Figure S5b, SI), and the leaching of Ru and Zr into the supernatant in each run was very minimal (Table S3, SI).

Control Experiments

Several control experiments were performed to understand the exclusivity of the single-site ruthenium dihydride species within MOFs. Ru-nanoparticles showed no selectivity in the hydrogenolysis of polyethylene (M_w ∼ 4000 Da, M_n ∼ 1700 Da) at 200 °C under 35 bar H$_2$ for 72 h (Figure 3d and section 3.1.5, SI). Ru(0)-nanoparticles encapsulated within the UiO-66 MOF (Ru@UiO-66) also showed less catalytic activity and poor selectivity than UiO-66-RuH$_2$. Under the identical reaction conditions and Ru-loading (4 μmol), Ru@UiO-66 depolymerized polyethylene in 49% conversion with 73% selectivity in C20−C35 alkanes (lubricant), whereas UiO-66-

RuH$_2$ gave 84% conversion with 78% selectivity in the liquid phase for C5−C12 alkanes (Figure 3d). The amount of H$_2$ consumption and the mass-specific catalytic activity (mol$_{H2}$ g$_{Ru}$$^{-1}$) were higher in the hydrogenolysis with UiO-66-RuH$_2$ than with Ru@UiO-66, suggesting a higher rate of C−C bond scission in UiO-66-Ru catalyzed hydrogenolysis of polyethylene (Figure S12, SI). We thus infer that the high selectivity of UiO-RuH$_2$ catalysts arises from not only the confinement of Ru-dihydride species within the well-defined and uniform porous MOF-structures but also the single-site nature of the Ru-active sites. UiO-66-RuH$_2$ catalyzed hydrogenolysis of polyethylene, performed in the presence of a drop of mercury,[93] was unaffected and yielded similar conversion and product distribution, suggesting that any ruthenium nanoparticles or any other leached metallic ruthenium particulates were not the active species in the reaction (Section 3.2.0, SI). The hydrogenolysis stopped after UiO-66-RuH$_2$ was removed from the reaction mixture, reinstating that the active catalytic species was embedded in the UiO MOF (Section 3.2.1, SI).

Mechanism Exploration of Hydrogenolysis of Polyethylene

The time evaluation for hydrogenolysis of LDPE (M_w = 150 kDa) over UiO-66-RuH$_2$ was studied to understand the relative rates of C−C bond scission at different positions along the paraffinic chains (Figure 6a). Methane and propane were produced exclusively in the first 2 h of the reaction when the conversion of LDPE was less than 5%. Upon progression of the reaction, the hydrocarbon product distribution readily shifted from paraffin to lower carbon numbers after 4 h, and the production of liquid hydrocarbons dominates over gas. After 24 h, liquid products were obtained in >90% selectivity with 50% LDPE conversion. This data suggests that the initial formation of methane and propane is likely due to the C−C bond dissociation toward the chain-ends upon diffusion of LDPE chains within the MOF pores. The activation of a C^2−H bond of a terminal linear polymer chain forms Ru[C^{2}H-(C^{1}H$_3$)(C^{3}H$_2$C^{4}H$_2$−P)] (P; polymer chain) intermediate, which undergoes β-C^{4}H$_2$−P elimination to generate propene.[7,94] Subsequently, UiO-Ru catalyzed hydrogenation of propene furnishes propane (Figure S20a, SI). Similarly, the activation of a C^3−H bond of the paraffinic chain forms Ru[C^{3}H(C^{2}H$_2$C^{1}H$_3$)(C^{4}H$_2$−P)], which undergoes β-C^{1}H$_3$ elimination, followed by the reaction with H$_2$ to produce CH$_4$ (Figure S20b, SI).

The hydrogenolysis of n-octadecane as a model of the linear alkane chain was performed under identical reaction conditions, which also showed significant production of methane and propane at the early stages of the reaction (Figure 6b). However, the rapid and selective formation of C10−C30 hydrocarbons during the course of the reaction indicates facile internal C−C bond hydrogenolysis of the polymer chain by UiO-66-RuH$_2$. We surmise that the coordinative unsaturated Ru center in UiO-RuH$_2$ facilitates the activation and cleavage of sterically hindered internal C−C bonds in paraffinic chains. To corroborate this hypothesis, we performed hydrogenolysis of 2,2,4,4,6,8,8-heptamethylnonane having different types of C−C bonds (Figure 6c). The analysis of the crude reaction mixture at ∼50% conversion showed the formation of 2,2,4-trimethyl pentane and 2,2,4,6-tetramethyl heptane as the major products via the dissociation of C$_{tertiary}$−C$_{secondary}$ bonds.
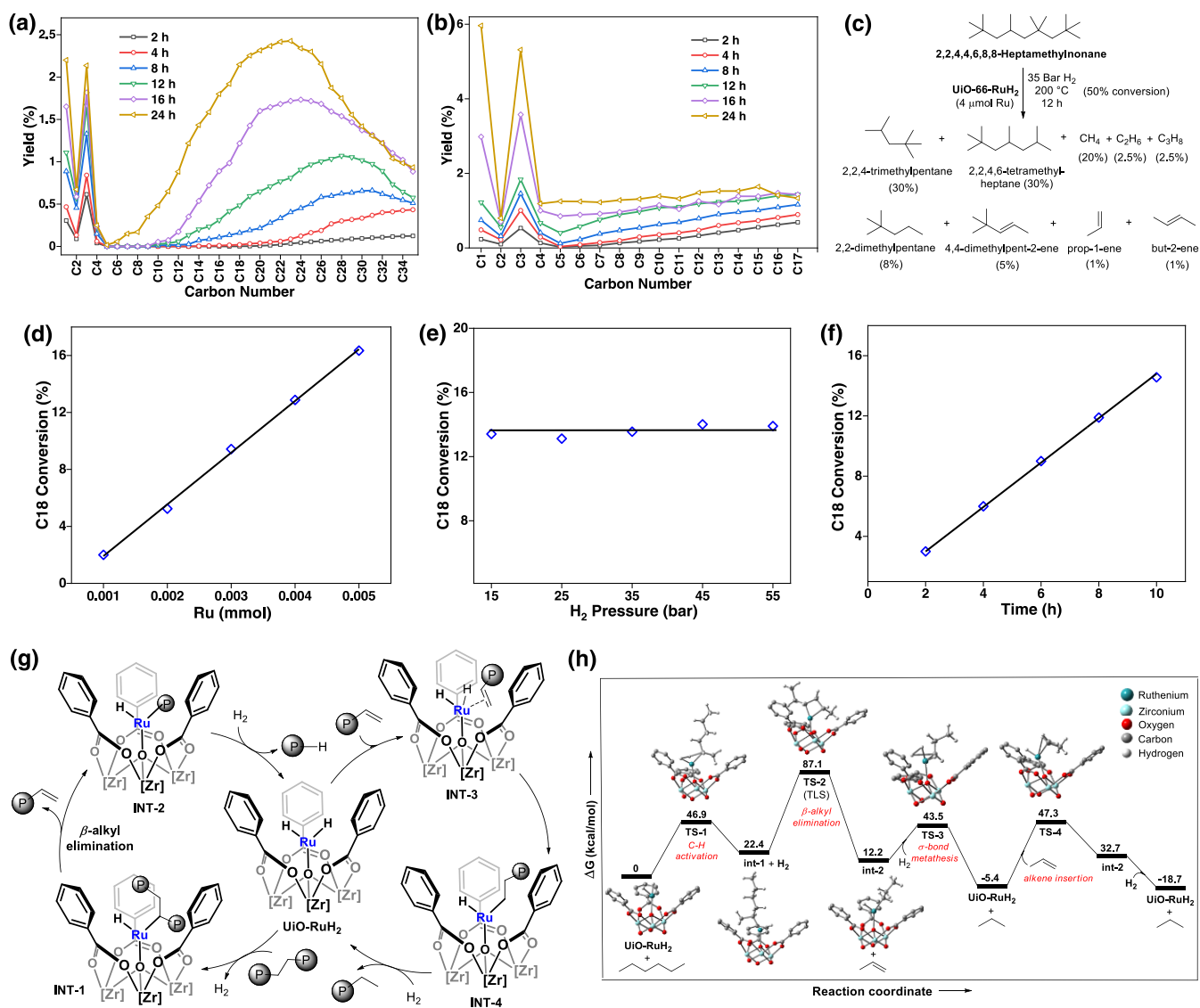
Figure 6. Time evaluation of nonsolid yields in the hydrogenolysis of (a) LDPE plastic bag and (b) n-octadecane over UiO-66-RuH$_2$ at 200 °C under 35 bar H$_2$. Reaction conditions: 0.60 g of LDPE plastic bag or n-octadecane, ~4 μmol of Ru, 200 °C, 35 bar H$_2$. (c) Products obtained after hydrogenolysis of 2,2,4,4,6,8,8-heptamethylnonane. (d–f) Kinetic data of n-octadecane (C18) hydrogenolysis as a function of reaction parameters. (d) %C18 conversion as a function of ruthenium loading. Reaction conditions: 0.60 g of C18, UiO-66-RuH$_2$ (0.001−0.005 mmol of Ru), 200 °C, 35 bar H$_2$, 9 h. (e) %C18 conversion as a function of H$_2$ pressure. Reaction conditions: 0.60 g of C18, UiO-66-RuH$_2$ (4 μmol of Ru), 200 °C, 9 h, 15−55 bar H$_2$. (f) %C18 Conversion as a function of reaction time. Reaction conditions: 0.60 g of C18, UiO-66-RuH$_2$ (4 μmol of Ru), 200 °C, 35 bar of H$_2$, 2−10 h. (g) Proposed catalytic cycle of UiO-RuH$_2$ catalyzed hydrogenolysis of polyethylene. (h) DFT-calculated free energy diagram at 473 K for UiO-RuH$_2$ catalyzed hydrogenolysis of hexane.

Metal-mediated polyolefin C−C bond cleavage primarily occurs via β-alkyl transfer[12,94] or σ-bond metathesis[95,96] in the turnover-limiting step (TLS). To further understand the UiO-Ru catalyzed hydrogenolysis pathways and examine the TLS, the empirical rate law of the reaction was determined using n-octadecane as a model substrate. The kinetics was performed by initial rate methods at low conversions (<16% conversion) of C18 to minimize the effect of small alkane invasion and hydrogen starvation.[97] The rate of conversion of n-octadecane showed a linear progression with the ruthenium loading (0.001−0.005 mmol) but was found to be independent of the H$_2$ pressure (15−55 bar) (Figures 6d-e). This implied a first-order dependence of the rate of hydrogenolysis on the ruthenium concentration and a zero-order dependence on the H$_2$ pressure. In addition, the plot of %C18 conversion vs time was linear, indicating that hydrogenolysis is pseudo-zero-order

with respect to the substrate (Figure 6f). From the empirical rate law, $r = k[\text{Ru}]^1[\text{C18}]^0[\text{H}_2]^0$, we infer that C18 and H$_2$ are not involved in the TLS or any preceding steps in rapid equilibrium. Based on the above experimental data, we propose that activation of a C−H bond in the polymer chain by Ru-dihydride forms a Ru-alkyl intermediate (INT-1) with liberation of H$_2$ via σ-bond metathesis (Figure 6g). Then, the turnover limiting β-alkyl elimination in INT-1 transforms to INT-2 bearing a polymer fragment and releases another fraction with a terminal double bond. In fact, several alkenes, such as hexene and octene, were detected by GC-MS during the time evaluation study for hydrogenolysis of LDPE. Then, the σ-bond metathesis between Ru-alkyl and H$_2$ furnishes short-chain alkane and regenerates the RuH$_2$ catalyst. RuH$_2$ further catalyzes the hydrogenation of the in situ generated alkene fragment to produce the corresponding alkane (Figure

6g). Our control experiment revealed that UiO-66-RuH$_2$ is also a highly active catalyst for the hydrogenation of alkenes (Section 3.2.3, SI), thus further supporting the proposed pathway. The empirical rate law further suggests that the σ-bond metathesis pathway, in which UiO-RuH$_2$ mediated C−C bond scission occurs via σ-bond metathesis, followed by regeneration of UiO-RuH$_2$ via σ-bond metathesis between Ru-alkyl intermediate and H$_2$, is unlikely, since both C18 and H$_2$ are not involved in the TLS.

Density Functional Theory (DFT) calculation was performed for UiO-RuH$_2$ catalyzed hydrogenolysis of hexane as the model substrate to propane at 473 K for investigating the low-energy pathway and the turnover limiting step (TLS). The energy profile diagram shows that β-alkyl transfer (int-1 → int-2) is the TLS, which has the higher activation barrier compared to those of other steps such as C−H activation via σ-bond metathesis (UiO-RuH$_2$ → int-1) and alkene insertion (UiO-RuH$_2$ → int-2) (Figure 6h). In addition, the polymer chain with the terminal double bond (propene in the calculation) is not strongly bonded to int-2 and thus easily desorbs from the MOF surface (Figure S22, SI). Moreover, β-hydride elimination of int-1 requires higher activation energy than β-alkyl elimination, making it kinetically unfavorable (Figure S22a, SI).[98] We also calculated the alternative σ-bond metathesis pathway (Figure S22b, SI). However, this σ-bond metathesis pathway has a higher barrier than the β-alkyl transfer pathway. Our kinetics and theoretical calculation suggest C−C bond scission involving β-alkyl transfer in the TLS.

CONCLUSIONS

The porous and isoreticular MOF-confined mononuclear Ru-dihydrides allow a systematic and target-centric approach toward the catalytic depolymerization of plastics. By tuning the pore sizes of the UiO-MOFs, the distribution of the short-chain hydrocarbon products could be systematically altered via shape-selective catalysis. A C12 centered narrow distribution of C8−C16 alkanes was obtained in >80% yield by the hydrogenolysis of single-use LPDE bags and droppers using UiO-66-RuH$_2$ with a very low Ru-loading, giving a LDPE to Ru weight ratio of 1485. The MOF-catalysts require no high-temperature preactivation and are recyclable at least 5 times. This work thus represents a state-of-the-art catalytic architecture employing MOFs to efficiently upcycle plastic wastes by combining the advantages of single-site nature of the Ru-center, uniform and tunable pores, well-defined porous structure, and superior stability via active site-isolation.

EXPERIMENTAL SECTION

UiO-RuH$_2$ MOF Synthesis

Synthesis of UiO-66-RuH$_2$. A 10 mL Teflon lined hydrothermal autoclave was charged with a solution of terephthalic acid (0.050 g, 0.304 mmol) and ZrCl$_4$ (69 mg, 0.296 mmol) in 2.4 mL of DMF and then heated at 120 °C for 24 h. After cooling to room temperature, the resultant white solid of UiO-66 MOF was isolated via centrifugation and washed with DMF and THF several times. n-BuLi (40 μL, 1.65 M in cyclohexane) was added to the slurry of UiO-66 MOF (17 mg, 0.010 mmol) in 1 mL of THF in a glovebox, and the mixture was slowly stirred for 2 h at room temperature. The MOF solid was washed with THF several times and then transferred to a 15 mL THF solution of RuCl$_3$·3H$_2$O (21 mg, 0.079 mmol). The mixture was stirred slowly for 6 h at room temperature. The resultant UiO-66-RuCl$_2$ MOF was separated from the suspension via centrifugation and

washed with THF and ethyl acetate several times over 7 days to remove the excess ruthenium. Inside the glovebox, NaEt$_3$BH (35 μL, 1 M in toluene) was added dropwise into a vial containing UiO-66-RuCl$_2$ (15.0 mg, 0.008 mmol) in 1 mL of THF, and the mixture was stirred gently at room temperature for 15 min. The resultant black solid of UiO-66-RuH$_2$ was separated via centrifugation and washed with THF. The 30% μ_3-OH group at SBUs was metalated with ruthenium ion as analyzed by ICP-OES of the digested MOF.

Synthesis of UiO-67-RuH$_2$. A 50 mg portion of biphenyl-4,4′-dicarboxylic acid dissolved in 1 mL of DMF was added to a solution of 69 mg of ZrCl$_4$ in 1 mL of DMF. The mixture was transferred into a 10 mL Teflon lined hydrothermal autoclave. The autoclaved was sealed and heated at 120 °C for 24 h. The resultant white solid of the UiO-67 MOF (21 mg, 0.010 mmol) was washed with THF multiple times and then treated with 40 μL of n-BuLi in THF at room temperature in a glovebox. After 2 h, the MOF solid was washed with THF and transferred to a 15 mL solution of RuCl$_3$.3H$_2$O (21 mg, 0.079 mmol). The slurry was slowly stirred for 6 h inside the glovebox. The resulting UiO-67-RuCl$_2$ was washed with THF and ethyl acetate over the next 7 days in the glovebox and then treated with NaEt$_3$BH (38 μL, 1 M in toluene) in 1 mL of THF. After 15 min at room temperature, the resultant black solid was separated via centrifugation and washed with THF and ethyl acetate several times to afford UiO-67-RuH$_2$. UiO-67-RuH$_2$ had 35% ruthenium loading with respect to μ_3-OH at SBUs as determined by the ICP-OES analysis of the digested MOF.

Synthesis of UiO-68-RuH$_2$. A 15 mL glass vial was charged with a 5 mL DMF solution of ZrCl$_4$ (26 mg, 0.11 mmol) and 1,4-bis(4-carboxyphenyl) benzene (53 mg, 0.17 mmol), followed by 31 μL of trifluoroacetic acid. The vial was capped and heated at 120 °C for 3 days. The resultant white precipitate of UiO-68 MOF was isolated via centrifugation and washed with DMF and THF. 40 uL of n-BuLi was added to a THF slurry of UiO-68 (26 mg, 0.010 mmol), and the mixture was slowly stirred for 2 h in the glovebox. After washing the solid MOF with THF, the MOF was stirred in a 15 mL of THF solution of RuCl$_3$.3H$_2$O (21 mg, 0.079 mmol) for 6 h to afford UiO-68-RuCl$_2$. The UiO-68-RuCl$_2$ (22 mg, 0.008 mmol) solid was washed with THF and then reacted with NaEt$_3$BH (38 μL, 1 M in toluene) in THF at room temperature for 15 min to afford UiO-68-RuH$_2$ as a black solid. ICP-OES analysis of the digested MOF revealed 33% Ru-loading with respect to μ_3-OH at the SBUs of UiO-68-RuH$_2$.

Procedure for UiO-RuH$_2$ Catalyzed Hydrogenolysis of Single-Use LDPE Plastics. A 100 mL nonstirred pressure vessel with a glass line was charged with 2.4 g of single-use LDPE plastic bag or dropper and UiO-RuH$_2$ catalyst (24−33 mg, 16 μmol of Ru) inside a glovebox. The reactor was sealed and purged with H$_2$ outside of the glovebox. The reactor was pressurized with 35 bar of hydrogen and then heated at 200 °C for 20 h. After the reaction, the reactor was cooled to 0 °C, and the gas was analyzed by GC-FID. The reactor was opened, and the solid MOF was separated from the liquid product via centrifugation. The liquid hydrocarbons were analyzed by GC-MS and quantified by GC-FID using 4-methylanisole as an internal standard. The yield of lubricants or wax products was determined by GPC of the crude products after catalysis.

ASSOCIATED CONTENT

Supporting Information

The Supporting Information is available free of charge at https://pubs.acs.org/doi/10.1021/jacsau.3c00633.

> Synthesis and characterization of UiO-RuH$_2$ catalysts, procedures and optimization of the hydrogenolysis of polymers, control experiments, details for X-ray absorption spectroscopic analysis and DFT calculations (PDF)

■ AUTHOR INFORMATION

Corresponding Author

Kuntal Manna − *Department of Chemistry, Indian Institute of Technology Delhi, Hauz Khas, New Delhi 110016, India;* ⊙ orcid.org/0000-0002-2924-0353; Email: kmanna@ chemistry.iitd.ac.in

Authors

Manav Chauhan − *Department of Chemistry, Indian Institute of Technology Delhi, Hauz Khas, New Delhi 110016, India*

Neha Antil − *Department of Chemistry, Indian Institute of Technology Delhi, Hauz Khas, New Delhi 110016, India*

Bharti Rana − *Department of Chemistry, Indian Institute of Technology Delhi, Hauz Khas, New Delhi 110016, India*

Naved Akhtar − *Department of Chemistry, Indian Institute of Technology Delhi, Hauz Khas, New Delhi 110016, India*

Chhaya Thadhani − *Department of Chemistry, Indian Institute of Technology Delhi, Hauz Khas, New Delhi 110016, India*

Wahida Begum − *Department of Chemistry, Indian Institute of Technology Delhi, Hauz Khas, New Delhi 110016, India*

Complete contact information is available at:
https://pubs.acs.org/10.1021/jacsau.3c00633

Author Contributions

CRediT: **Manav Chauhan** data curation, formal analysis, investigation, methodology, writing-original draft; **Neha Antil** formal analysis, investigation; **Bharti Rana** formal analysis, investigation, methodology; **Naved Akhtar** data curation, formal analysis, software; **Chhaya Thadhani** investigation, methodology; **Wahida Begum** investigation, methodology; **Kuntal Manna** conceptualization, formal analysis, funding acquisition, investigation, resources, supervision, writing-original draft.

Notes

The authors declare no competing financial interest.

■ REFERENCES

(1) Plastic Market Size, Share & Trends Analysis Report By Product (PE, PP, PU, PVC, PET, Polystyrene, ABS, PBT, PPO, Epoxy Polymers, LCP, PC, Polyamide), By Application, By End Use, And Segment Forecasts, 2022−2030. Research and Markets. https://www.researchandmarkets.com/reports/4751797/plastic-market-size-share-and-trends-analysis (accessed 2022-05-14).

(2) Chen, H.; Wan, K.; Zhang, Y.; Wang, Y. Waste to Wealth: Chemical Recycling and Chemical Upcycling of Waste Plastics for a Great Future. *ChemSusChem* **2021**, *14* (19), 4123−4136.

(3) Geyer, R.; Jambeck, J. R.; Law, K. L. Production, use, and fate of all plastics ever made. *Sci. Adv.* **2017**, *3* (7), No. e1700782.

(4) Martín, A. J.; Mondelli, C.; Jaydev, S. D.; Pérez-Ramírez, J. Catalytic processing of plastic waste on the rise. *Chem.* **2021**, *7* (6), 1487−1533.

(5) Maugh, T. H. Incineration, Deep Wells Gain New Importance. *Science* **1979**, *204* (4398), 1188−1190.

(6) Zhou, S.; Liu, C.; Zhang, L. Critical Review on the Chemical Reaction Pathways Underpinning the Primary Decomposition Behavior of Chlorine-Bearing Compounds under Simulated Municipal Solid Waste Incineration Conditions. *Energy Fuels* **2020**, *34* (1), 1−15.

(7) Cho, S.; Kim, J. Cost Saving of the Explosive Waste Incineration Process via an Optimal Heat Exchanger Network. *ACS Omega* **2022**, *7* (22), 18681−18687.

(8) Liu, S.; Kots, P. A.; Vance, B. C.; Danielson, A.; Vlachos, D. G. Plastic waste to fuels by hydrocracking at mild conditions. *Sci. Adv.* **2021**, *7* (17), No. eabf8283.

(9) Duan, J.; Chen, W.; Wang, C.; Wang, L.; Liu, Z.; Yi, X.; Fang, W.; Wang, H.; Wei, H.; Xu, S.; Yang, Y.; Yang, Q.; Bao, Z.; Zhang, Z.; Ren, Q.; Zhou, H.; Qin, X.; Zheng, A.; Xiao, F.-S. Coking-Resistant Polyethylene Upcycling Modulated by Zeolite Micropore Diffusion. *J. Am. Chem. Soc.* **2022**, *144* (31), 14269−14277.

(10) Fu, L.; Xiong, Q.; Wang, Q.; Cai, L.; Chen, Z.; Zhou, Y. Catalytic Pyrolysis of Waste Polyethylene Using Combined CaO and Ga/ZSM-5 Catalysts for High Value-Added Aromatics Production. *ACS Sustain. Chem. Eng.* **2022**, *10* (29), 9612−9623.

(11) Kots, P. A.; Vance, B. C.; Vlachos, D. G. Polyolefin plastic waste hydroconversion to fuels, lubricants, and waxes: a comparative study. *React. Chem. Eng.* **2021**, *7* (1), 41−54.

(12) Dufaud, V.; Basset, J.-M. Catalytic Hydrogenolysis at Low Temperature and Pressure of Polyethylene and Polypropylene to Diesels or Lower Alkanes by a Zirconium Hydride Supported on Silica-Alumina: A Step Toward Polyolefin Degradation by the Microscopic Reverse of Ziegler-Natta Polymerization. *Angew. Chem., Int. Ed.* **1998**, *37* (6), 806−810.

(13) Jaydev, S. D.; Martín, A. J.; Pérez-Ramírez, J. Direct Conversion of Polypropylene into Liquid Hydrocarbons on Carbon-Supported Platinum Catalysts. *ChemSusChem* **2021**, *14* (23), 5179−5185.

(14) Celik, G.; Kennedy, R. M.; Hackler, R. A.; Ferrandon, M.; Tennakoon, A.; Patnaik, S.; LaPointe, A. M.; Ammal, S. C.; Heyden, A.; Perras, F. A.; Pruski, M.; Scott, S. L.; Poeppelmeier, K. R.; Sadow, A. D.; Delferro, M. Upcycling Single-Use Polyethylene into High-Quality Liquid Products. *ACS Cent. Sci.* **2019**, *5* (11), 1795−1803.

(15) Hackler, R. A.; Vyavhare, K.; Kennedy, R. M.; Celik, G.; Kanbur, U.; Griffin, P. J.; Sadow, A. D.; Zang, G.; Elgowainy, A.; Sun, P.; Poeppelmeier, K. R.; Erdemir, A.; Delferro, M. Synthetic Lubricants Derived from Plastic Waste and their Tribological Performance. *ChemSusChem* **2021**, *14* (19), 4181−4189.

(16) Tennakoon, A.; Wu, X.; Paterson, A. L.; Patnaik, S.; Pei, Y.; LaPointe, A. M.; Ammal, S. C.; Hackler, R. A.; Heyden, A.; Slowing, I. I.; Coates, G. W.; Delferro, M.; Peters, B.; Huang, W.; Sadow, A. D.; Perras, F. A. Catalytic upcycling of high-density polyethylene via a processive mechanism. *Nat. Catal.* **2020**, *3* (11), 893−901.

(17) Zhang, F.; Zeng, M.; Yappert, R. D.; Sun, J.; Lee, Y.-H.; LaPointe, A. M.; Peters, B.; Abu-Omar, M. M.; Scott, S. L. Polyethylene upcycling to long-chain alkylaromatics by tandem hydrogenolysis/aromatization. *Science* **2020**, *370* (6515), 437−441.

(18) Rorrer, J. E.; Beckham, G. T.; Román-Leshkov, Y. Conversion of Polyolefin Waste to Liquid Alkanes with Ru-Based Catalysts under Mild Conditions. *JACS Au* **2021**, *1* (1), 8−12.

(19) Jia, C.; Xie, S.; Zhang, W.; Intan, N. N.; Sampath, J.; Pfaendtner, J.; Lin, H. Deconstruction of high-density polyethylene into liquid hydrocarbon fuels and lubricants by hydrogenolysis over Ru catalyst. *Chem. Catal.* **2021**, *1* (2), 437−455.

(20) Rorrer, J. E.; Troyano-Valls, C.; Beckham, G. T.; Román-Leshkov, Y. Hydrogenolysis of Polypropylene and Mixed Polyolefin Plastic Waste over Ru/C to Produce Liquid Alkanes. *ACS Sustain. Chem. Eng.* **2021**, *9* (35), 11661−11666.

(21) Chen, L.; Zhu, Y.; Meyer, L. C.; Hale, L. V.; Le, T. T.; Karkamkar, A.; Lercher, J. A.; Gutiérrez, O. Y.; Szanyi, J. Effect of reaction conditions on the hydrogenolysis of polypropylene and polyethylene into gas and liquid alkanes. *React. Chem. Eng.* 2022, 7 (4), 844−854.

(22) Nakaji, Y.; Tamura, M.; Miyaoka, S.; Kumagai, S.; Tanji, M.; Nakagawa, Y.; Yoshioka, T.; Tomishige, K. Low-temperature catalytic upgrading of waste polyolefinic plastics into liquid fuels and waxes. *Appl. Catal., B* 2021, 285, 119805.

(23) Kots, P. A.; Liu, S.; Vance, B. C.; Wang, C.; Sheehan, J. D.; Vlachos, D. G. Polypropylene Plastic Waste Conversion to Lubricants over Ru/TiO$_2$ Catalysts. *ACS Catal.* 2021, 11 (13), 8104−8115.

(24) Wang, C.; Xie, T.; Kots, P. A.; Vance, B. C.; Yu, K.; Kumar, P.; Fu, J.; Liu, S.; Tsilomelekis, G.; Stach, E. A.; Zheng, W.; Vlachos, D. G. Polyethylene Hydrogenolysis at Mild Conditions over Ruthenium on Tungstated Zirconia. *JACS Au* 2021, 1 (9), 1422−1434.

(25) Chen, S.; Tennakoon, A.; You, K.-E.; Paterson, A. L.; Yappert, R.; Alayoglu, S.; Fang, L.; Wu, X.; Zhao, T. Y.; Lapak, M. P.; Saravanan, M.; Hackler, R. A.; Wang, Y.-Y.; Qi, L.; Delferro, M.; Li, T.; Lee, B.; Peters, B.; Poeppelmeier, K. R.; Ammal, S. C.; Bowers, C. R.; Perras, F. A.; Heyden, A.; Sadow, A. D.; Huang, W. Ultrasmall amorphous zirconia nanoparticles catalyse polyolefin hydrogenolysis. *Nat. Catal.* 2023, 6 (2), 161−173.

(26) Ono, Y. Transformation of Lower Alkanes into Aromatic Hydrocarbons over ZSM-5 Zeolites. *Catal. Rev.: Sci. Eng.* 1992, 34 (3), 179−226.

(27) Bhan, A.; Nicholas Delgass, W. Propane Aromatization over HZSM-5 and Ga/HZSM-5 Catalysts. *Catal. Rev.: Sci. Eng.* 2008, 50 (1), 19−151.

(28) Rahimi, N.; Karimzadeh, R. Catalytic cracking of hydrocarbons over modified ZSM-5 zeolites to produce light olefins: A review. *Appl. Catal., A* 2011, 398 (1), 1−17.

(29) Shi, J.; Wang, Y.; Yang, W.; Tang, Y.; Xie, Z. Recent advances of pore system construction in zeolite-catalyzed chemical industry processes. *Chem. Soc. Rev.* 2015, 44 (24), 8877−8903.

(30) Wang, L.; Wang, G.; Zhang, J.; Bian, C.; Meng, X.; Xiao, F.-S. Controllable cyanation of carbon-hydrogen bonds by zeolite crystals over manganese oxide catalyst. *Nat. Commun.* 2017, 8 (1), 15240.

(31) Arudra, P.; Bhuiyan, T. I.; Akhtar, M. N.; Aitani, A. M.; Al-Khattaf, S. S.; Hattori, H. Silicalite-1 As Efficient Catalyst for Production of Propene from 1-Butene. *ACS Catal.* 2014, 4 (11), 4205−4214.

(32) Huang, H.-w.; Zhang, M.-x.; Chen, C.; Li, C.-y.; Cui, Q.-k. Catalytic performance of cerium modified Silicalite-1 molecular sieves in the conversion of methanol to propene. *J. Fuel Chem. Technol.* 2016, 44 (12), 1485−1493.

(33) Niu, X.; Li, X.; Yuan, G.; Feng, F.; Wang, M.; Zhang, X.; Wang, Q. Hollow Hierarchical Silicalite-1 Zeolite Encapsulated PtNi Bimetals for Selective Hydroconversion of Methyl Stearate into Aviation Fuel Range Alkanes. *Ind. Eng. Chem. Res.* 2020, 59 (18), 8601−8611.

(34) Li, X.; Wang, L.; Zhang, B.; Khajeh, A.; Shahbazi, A. Iron oxide supported on silicalite-1 as a multifunctional material for biomass chemical looping gasification and syngas upgrading. *J. Chem. Eng.* 2020, 401, 125943.

(35) Giordano, G.; Migliori, M.; Ferrarelli, G.; Giorgianni, G.; Dalena, F.; Peng, P.; Debost, M.; Boullay, P.; Liu, Z.; Guo, H.; Yan, Z.-F.; Mintova, S. Passivated Surface of High Aluminum Containing ZSM-5 by Silicalite-1: Synthesis and Application in Dehydration Reaction. *ACS Sustain. Chem. Eng.* 2022, 10 (15), 4839−4848.

(36) Wu, X.; Tennakoon, A.; Yappert, R.; Esveld, M.; Ferrandon, M. S.; Hackler, R. A.; LaPointe, A. M.; Heyden, A.; Delferro, M.; Peters, B.; Sadow, A. D.; Huang, W. Size-Controlled Nanoparticles Embedded in a Mesoporous Architecture Leading to Efficient and Selective Hydrogenolysis of Polyolefins. *J. Am. Chem. Soc.* 2022, 144 (12), 5323−5334.

(37) Cohen, S. M. Postsynthetic Methods for the Functionalization of Metal-Organic Frameworks. *Chem. Rev.* 2012, 112 (2), 970−1000.

(38) Genna, D. T.; Wong-Foy, A. G.; Matzger, A. J.; Sanford, M. S. Heterogenization of Homogeneous Catalysts in Metal-Organic Frameworks via Cation Exchange. *J. Am. Chem. Soc.* 2013, 135 (29), 10586−10589.

(39) Gascon, J.; Corma, A.; Kapteijn, F.; Llabrés i Xamena, F. X. Metal Organic Framework Catalysis: Quo vadis? *ACS Catal.* 2014, 4 (2), 361−378.

(40) Rimoldi, M.; Howarth, A. J.; DeStefano, M. R.; Lin, L.; Goswami, S.; Li, P.; Hupp, J. T.; Farha, O. K. Catalytic Zirconium/ Hafnium-Based Metal-Organic Frameworks. *ACS Catal.* 2017, 7 (2), 997−1014.

(41) Yang, D.; Odoh, S. O.; Wang, T. C.; Farha, O. K.; Hupp, J. T.; Cramer, C. J.; Gagliardi, L.; Gates, B. C. Metal-Organic Framework Nodes as Nearly Ideal Supports for Molecular Catalysts: NU-1000- and UiO-66-Supported Iridium Complexes. *J. Am. Chem. Soc.* 2015, 137 (23), 7391−7396.

(42) Manna, K.; Ji, P.; Greene, F. X.; Lin, W. Metal-Organic Framework Nodes Support Single-Site Magnesium-Alkyl Catalysts for Hydroboration and Hydroamination Reactions. *J. Am. Chem. Soc.* 2016, 138 (24), 7488−7491.

(43) Liu, J.; Ye, J.; Li, Z.; Otake, K.-i.; Liao, Y.; Peters, A. W.; Noh, H.; Truhlar, D. G.; Gagliardi, L.; Cramer, C. J.; Farha, O. K.; Hupp, J. T. Beyond the Active Site: Tuning the Activity and Selectivity of a Metal-Organic Framework-Supported Ni Catalyst for Ethylene Dimerization. *J. Am. Chem. Soc.* 2018, 140 (36), 11174−11178.

(44) Park, H. D.; Dincă, M.; Román-Leshkov, Y. Continuous-Flow Production of Succinic Anhydrides via Catalytic β-Lactone Carbonylation by Co(CO)$_4$⊂Cr-MIL-101. *J. Am. Chem. Soc.* 2018, 140 (34), 10669−10672.

(45) Han, Q.; He, C.; Zhao, M.; Qi, B.; Niu, J.; Duan, C. Engineering Chiral Polyoxometalate Hybrid Metal-Organic Frameworks for Asymmetric Dihydroxylation of Olefins. *J. Am. Chem. Soc.* 2013, 135 (28), 10186−10189.

(46) Xiao, D. J.; Bloch, E. D.; Mason, J. A.; Queen, W. L.; Hudson, M. R.; Planas, N.; Borycz, J.; Dzubak, A. L.; Verma, P.; Lee, K.; Bonino, F.; Crocellà, V.; Yano, J.; Bordiga, S.; Truhlar, D. G.; Gagliardi, L.; Brown, C. M.; Long, J. R. Oxidation of ethane to ethanol by N$_2$O in a metal-organic framework with coordinatively unsaturated iron(II) sites. *Nat. Chem.* 2014, 6 (7), 590−595.

(47) Gonzalez, M. I.; Bloch, E. D.; Mason, J. A.; Teat, S. J.; Long, J. R. Single-Crystal-to-Single-Crystal Metalation of a Metal-Organic Framework: A Route toward Structurally Well-Defined Catalysts. *Inorg. Chem.* 2015, 54 (6), 2995−3005.

(48) Kutzscher, C.; Hoffmann, H. C.; Krause, S.; Stoeck, U.; Senkovska, I.; Brunner, E.; Kaskel, S. Proline Functionalization of the Mesoporous Metal-Organic Framework DUT-32. *Inorg. Chem.* 2015, 54 (3), 1003−1009.

(49) Kutzscher, C.; Nickerl, G.; Senkovska, I.; Bon, V.; Kaskel, S. Proline Functionalized UiO-67 and UiO-68 Type Metal-Organic Frameworks Showing Reversed Diastereoselectivity in Aldol Addition Reactions. *Chem. Mater.* 2016, 28 (8), 2573−2580.

(50) Xia, Q.; Li, Z.; Tan, C.; Liu, Y.; Gong, W.; Cui, Y. Multivariate Metal-Organic Frameworks as Multifunctional Heterogeneous Asymmetric Catalysts for Sequential Reactions. *J. Am. Chem. Soc.* 2017, 139 (24), 8259−8266.

(51) Metzger, E. D.; Comito, R. J.; Hendon, C. H.; Dincă, M. Mechanism of Single-Site Molecule-Like Catalytic Ethylene Dimerization in Ni-MFU-4l. *J. Am. Chem. Soc.* 2017, 139 (2), 757−762.

(52) Li, X.; Zhang, B.; Tang, L.; Goh, T. W.; Qi, S.; Volkov, A.; Pei, Y.; Qi, Z.; Tsung, C.-K.; Stanley, L.; Huang, W. Cooperative Multifunctional Catalysts for Nitrone Synthesis: Platinum Nanoclusters in Amine-Functionalized Metal-Organic Frameworks. *Angew. Chem., Int. Ed.* 2017, 56 (51), 16371−16375.

(53) Dunning, S. G.; Reynolds, J. E.; Walsh, K. M.; Kristek, D. J.; Lynch, V. M.; Kunal, P.; Humphrey, S. M. Direct, One-Pot Syntheses of MOFs Decorated with Low-Valent Metal-Phosphine Complexes. *Organometallics* 2019, 38 (18), 3406−3411.

(54) Zhang, Y.; Li, J.; Yang, X.; Zhang, P.; Pang, J.; Li, B.; Zhou, H.-C. A mesoporous NNN-pincer-based metal-organic framework

scaffold for the preparation of noble-metal-free catalysts. *Chem. Commun.* **2019**, 55 (14), 2023−2026.

(55) Wisser, F. M.; Duguet, M.; Perrinet, Q.; Ghosh, A. C.; Alves-Favaro, M.; Mohr, Y.; Lorentz, C.; Quadrelli, E. A.; Palkovits, R.; Farrusseng, D.; Mellot-Draznieks, C.; de Waele, V.; Canivet, J. Molecular Porous Photosystems Tailored for Long-Term Photocatalytic CO$_2$ Reduction. *Angew. Chem., Int. Ed.* **2020**, 59 (13), 5116−5122.

(56) Canivet, J.; Bernoud, E.; Bonnefoy, J.; Legrand, A.; Todorova, T. K.; Quadrelli, E. A.; Mellot-Draznieks, C. Synthetic and computational assessment of a chiral metal-organic framework catalyst for predictive asymmetric transformation. *Chem. Sci.* **2020**, 11 (33), 8800−8808.

(57) Seo, J. S.; Whang, D.; Lee, H.; Jun, S. I.; Oh, J.; Jeon, Y. J.; Kim, K. A homochiral metal-organic porous material for enantioselective separation and catalysis. *Nature* **2000**, 404 (6781), 982−986.

(58) Zhou, T.-Y.; Auer, B.; Lee, S. J.; Telfer, S. G. Catalysts Confined in Programmed Framework Pores Enable New Transformations and Tune Reaction Efficiency and Selectivity. *J. Am. Chem. Soc.* **2019**, 141 (4), 1577−1582.

(59) Sun, C.-Y.; Liu, S.-X.; Liang, D.-D.; Shao, K.-Z.; Ren, Y.-H.; Su, Z.-M. Highly Stable Crystalline Catalysts Based on a Microporous Metal-Organic Framework and Polyoxometalates. *J. Am. Chem. Soc.* **2009**, 131 (5), 1883−1888.

(60) Toyao, T.; Miyahara, K.; Fujiwaki, M.; Kim, T.-H.; Dohshi, S.; Horiuchi, Y.; Matsuoka, M. Immobilization of Cu Complex into Zr-Based MOF with Bipyridine Units for Heterogeneous Selective Oxidation. *J. Phys. Chem. C* **2015**, 119 (15), 8131−8137.

(61) Liu, Y.; Xuan, W.; Cui, Y. Engineering Homochiral Metal-Organic Frameworks for Heterogeneous Asymmetric Catalysis and Enantioselective Separation. *Adv. Mater.* **2010**, 22 (37), 4112−4135.

(62) Dang, D.; Wu, P.; He, C.; Xie, Z.; Duan, C. Homochiral Metal-Organic Frameworks for Heterogeneous Asymmetric Catalysis. *J. Am. Chem. Soc.* **2010**, 132 (41), 14321−14323.

(63) Kalaj, M.; Cohen, S. M. Postsynthetic Modification: An Enabling Technology for the Advancement of Metal-Organic Frameworks. *ACS Cent. Sci.* **2020**, 6 (7), 1046−1057.

(64) Fei, H.; Cohen, S. M. Metalation of a Thiocatechol-Functionalized Zr(IV)-Based Metal-Organic Framework for Selective C-H Functionalization. *J. Am. Chem. Soc.* **2015**, 137 (6), 2191−2194.

(65) Wu, Y.; Wang, X.; Kirlikovali, K. O.; Gong, X.; Atilgan, A.; Ma, K.; Schweitzer, N. M.; Gianneschi, N. C.; Li, Z.; Zhang, X.; Farha, O. K. Catalytic Degradation of Polyethylene Terephthalate Using a Phase-Transitional Zirconium-Based Metal-Organic Framework. *Angew. Chem., Int. Ed.* **2022**, 61 (24), No. e202117528.

(66) Antil, N.; Akhtar, N.; Newar, R.; Begum, W.; Kumar, A.; Chauhan, M.; Manna, K. Chiral Iron(II)-Catalysts within Valinol-Grafted Metal-Organic Frameworks for Enantioselective Reduction of Ketones. *ACS Catal.* **2021**, 11 (16), 10450−10459.

(67) Newar, R.; Akhtar, N.; Antil, N.; Kumar, A.; Shukla, S.; Begum, W.; Manna, K. Amino Acid-Functionalized Metal-Organic Frameworks for Asymmetric Base-Metal Catalysis. *Angew. Chem., Int. Ed.* **2021**, 60 (19), 10964−10970.

(68) Newar, R.; Begum, W.; Antil, N.; Shukla, S.; Kumar, A.; Akhtar, N.; Balendra; Manna, K. Single-Site Cobalt-Catalyst Ligated with Pyridylimine-Functionalized Metal-Organic Frameworks for Arene and Benzylic Borylation. *Inorg. Chem.* **2020**, 59 (15), 10473−10481.

(69) Sahoo, R.; Mondal, S.; Chand, S.; Das, M. C. Highly Robust Metal-Organic Framework for Efficiently Catalyzing Knoevenagel Condensation and the Strecker Reaction under Solvent-Free Conditions. *Inorg. Chem.* **2023**, 62 (32), 12989−13000.

(70) Pramanik, B.; Sahoo, R.; Das, M. C. pH-stable MOFs: Design principles and applications. *Coord. Chem. Rev.* **2023**, 493, 215301.

(71) Antil, N.; Kumar, A.; Akhtar, N.; Newar, R.; Begum, W.; Dwivedi, A.; Manna, K. Aluminum Metal-Organic Framework-Ligated Single-Site Nickel(II)-Hydride for Heterogeneous Chemoselective Catalysis. *ACS Catal.* **2021**, 11 (7), 3943−3957.

(72) Horike, S.; Dincă, M.; Tamaki, K.; Long, J. R. Size-Selective Lewis Acid Catalysis in a Microporous Metal-Organic Framework

with Exposed Mn2+ Coordination Sites. *J. Am. Chem. Soc.* **2008**, 130 (18), 5854−5855.

(73) Roberts, J. M.; Fini, B. M.; Sarjeant, A. A.; Farha, O. K.; Hupp, J. T.; Scheidt, K. A. Urea Metal-Organic Frameworks as Effective and Size-Selective Hydrogen-Bond Catalysts. *J. Am. Chem. Soc.* **2012**, 134 (7), 3334−3337.

(74) Zhang, W.; Lu, G.; Cui, C.; Liu, Y.; Li, S.; Yan, W.; Xing, C.; Chi, Y. R.; Yang, Y.; Huo, F. A Family of Metal-Organic Frameworks Exhibiting Size-Selective Catalysis with Encapsulated Noble-Metal Nanoparticles. *Adv. Mater.* **2014**, 26 (24), 4056−4060.

(75) Luz, I.; Rösler, C.; Epp, K.; Llabrés i Xamena, F. X.; Fischer, R. A. Pd@UiO-66-Type MOFs Prepared by Chemical Vapor Infiltration as Shape-Selective Hydrogenation Catalysts. *Eur. J. Inorg. Chem.* **2015**, 2015 (23), 3904−3912.

(76) Yang, L.; Cai, P.; Zhang, L.; Xu, X.; Yakovenko, A. A.; Wang, Q.; Pang, J.; Yuan, S.; Zou, X.; Huang, N.; Huang, Z.; Zhou, H.-C. Ligand-Directed Conformational Control over Porphyrinic Zirconium Metal-Organic Frameworks for Size-Selective Catalysis. *J. Am. Chem. Soc.* **2021**, 143 (31), 12129−12137.

(77) Manna, K.; Ji, P.; Lin, Z.; Greene, F. X.; Urban, A.; Thacker, N. C.; Lin, W. Chemoselective single-site Earth-abundant metal catalysts at metal-organic framework nodes. *Nat. Commun.* **2016**, 7 (1), 12610.

(78) Ji, P.; Manna, K.; Lin, Z.; Urban, A.; Greene, F. X.; Lan, G.; Lin, W. Single-Site Cobalt Catalysts at New Zr$_8$(μ_2-O)$_8$(μ_2-OH)$_4$ Metal-Organic Framework Nodes for Highly Active Hydrogenation of Alkenes, Imines, Carbonyls, and Heterocycles. *J. Am. Chem. Soc.* **2016**, 138 (37), 12234−12242.

(79) Ji, P.; Manna, K.; Lin, Z.; Feng, X.; Urban, A.; Song, Y.; Lin, W. Single-Site Cobalt Catalysts at New Zr$_{12}$(μ_3-O)$_8$(μ_3-OH)$_8$(μ_2-OH)$_6$ Metal-Organic Framework Nodes for Highly Active Hydrogenation of Nitroarenes, Nitriles, and Isocyanides. *J. Am. Chem. Soc.* **2017**, 139 (20), 7004−7011.

(80) Song, Y.; Feng, X.; Chen, J. S.; Brzezinski, C.; Xu, Z.; Lin, W. Multistep Engineering of Synergistic Catalysts in a Metal-Organic Framework for Tandem C-O Bond Cleavage. *J. Am. Chem. Soc.* **2020**, 142 (10), 4872−4882.

(81) Wei, Y.-S.; Zhang, M.; Zou, R.; Xu, Q. Metal-Organic Framework-Based Catalysts with Single Metal Sites. *Chem. Rev.* **2020**, 120 (21), 12089−12174.

(82) Huang, H.; Shen, K.; Chen, F.; Li, Y. Metal-Organic Frameworks as a Good Platform for the Fabrication of Single-Atom Catalysts. *ACS Catal.* **2020**, 10 (12), 6579−6586.

(83) Yousuf, M. R.; Johnson, E. M.; Maynes, A. J.; Johnston, C. R.; Karim, A. M.; Morris, A. J.; Morris, J. R.; Troya, D. Catalytic CO Oxidation by Cu Single Atoms on the UiO-66 Metal-Organic Framework: The Role of the Oxidation State. *J. Phys. Chem. C* **2022**, 126 (30), 12507−12518.

(84) Fan, S.-C.; Chen, S.-Q.; Wang, J.-W.; Li, Y.-P.; Zhang, P.; Wang, Y.; Yuan, W.; Zhai, Q.-G. Precise Introduction of Single Vanadium Site into Indium-Organic Framework for CO$_2$ Capture and Photocatalytic Fixation. *Inorg. Chem.* **2022**, 61 (35), 14131−14139.

(85) Antil, N.; Chauhan, M.; Akhtar, N.; Kalita, R.; Manna, K. Selective Methane Oxidation to Acetic Acid Using Molecular Oxygen over a Mono-Copper Hydroxyl Catalyst. *J. Am. Chem. Soc.* **2023**, 145 (11), 6156−6165.

(86) Antil, N.; Chauhan, M.; Akhtar, N.; Newar, R.; Begum, W.; Malik, J.; Manna, K. Metal-Organic Framework-Encaged Monomeric Cobalt(III) Hydroperoxides Enable Chemoselective Methane Oxidation to Methanol. *ACS Catal.* **2022**, 12 (18), 11159−11168.

(87) Newar, R.; Kalita, R.; Akhtar, N.; Antil, N.; Chauhan, M.; Manna, K. N-Formylation of amines utilizing CO$_2$ by a heterogeneous metal-organic framework supported single-site cobalt catalyst. *Catal. Sci. Technol.* **2022**, 12 (22), 6795−6804.

(88) Antil, N.; Kumar, A.; Akhtar, N.; Newar, R.; Begum, W.; Manna, K. Metal-Organic Framework-Confined Single-Site Base-Metal Catalyst for Chemoselective Hydrodeoxygenation of Carbonyls and Alcohols. *Inorg. Chem.* **2021**, 60 (12), 9029−9039.

(89) Cavka, J. H.; Jakobsen, S.; Olsbye, U.; Guillou, N.; Lamberti, C.; Bordiga, S.; Lillerud, K. P. A New Zirconium Inorganic Building

Brick Forming Metal Organic Frameworks with Exceptional Stability. *J. Am. Chem. Soc.* **2008**, *130* (42), 13850−13851.

(90) Schaate, A.; Roy, P.; Godt, A.; Lippke, J.; Waltz, F.; Wiebcke, M.; Behrens, P. Modulated Synthesis of Zr-Based Metal-Organic Frameworks: From Nano to Single Crystals. *Chem.—Eur. J.* **2011**, *17* (24), 6643−6651.

(91) Valenzano, L.; Civalleri, B.; Chavan, S.; Bordiga, S.; Nilsen, M. H.; Jakobsen, S.; Lillerud, K. P.; Lamberti, C. Disclosing the Complex Structure of UiO-66 Metal Organic Framework: A Synergic Combination of Experiment and Theory. *Chem. Mater.* **2011**, *23* (7), 1700−1718.

(92) Yang, Q.; Zhang, H.-Y.; Wang, L.; Zhang, Y.; Zhao, J. Ru/UiO-66 Catalyst for the Reduction of Nitroarenes and Tandem Reaction of Alcohol Oxidation/Knoevenagel Condensation. *ACS Omega* **2018**, *3* (4), 4199−4212.

(93) Liu, Z.; Sriram, V.; Lee, J.-Y. Heterogeneous oxidation of elemental mercury vapor over RuO_2/rutile TiO_2 catalyst for mercury emissions control. *Appl. Catal., B* **2017**, *207*, 143−152.

(94) O'Reilly, M. E.; Dutta, S.; Veige, A. S. β-Alkyl Elimination: Fundamental Principles and Some Applications. *Chem. Rev.* **2016**, *116* (14), 8105−8145.

(95) Labinger, J. A.; Bercaw, J. E. Understanding and exploiting C-H bond activation. *Nature* **2002**, *417* (6888), 507−514.

(96) Waterman, R. σ-Bond Metathesis: A 30-Year Retrospective. *Organometallics* **2013**, *32* (24), 7249−7263.

(97) Mason, A. H.; Motta, A.; Das, A.; Ma, Q.; Bedzyk, M. J.; Kratish, Y.; Marks, T. J. Rapid atom-efficient polyolefin plastics hydrogenolysis mediated by a well-defined single-site electrophilic/cationic organo-zirconium catalyst. *Nat. Commun.* **2022**, *13* (1), 7187.

(98) Mortensen, J. J.; Parrinello, M. A Density Functional Theory Study of a Silica-Supported Zirconium Monohydride Catalyst for Depolymerization of Polyethylene. *J. Phys. Chem. B* **2000**, *104* (13), 2901−2907.